Cover sheet for: *The influence of orbital parameters on the North American Monsoon system during the Last Interglacial Period*

Nadja Insel
Northeastern Illinois University, Department of Earth Science
University of Chicago, Department of Geophysical Sciences

Max Berkelhammer
University of Illinois at Chicago, Department of Earth and Environmental Sciences

This manuscript has been peer-reviewed and published by the Journal of Quaternary Science, doi: 10.1002/jqs.3311

Please feel free to contact the authors for any matters relating to this manuscript.

The influence of orbital parameters on the North American Monsoon system during the Last Interglacial Period

Nadja Insel[1], Max Berkelhammer[2]
[1]Northeastern Illinois University, Department of Earth Science
[2]University of Illinois at Chicago, Department of Earth and Environmental Sciences

Abstract

The response of summer precipitation in the western U.S. to climate variability remains a subject of uncertainty. For example, paleoclimate records indicate the North American monsoon (NAM) was stronger and spatially more extensive during the Holocene, whereas recent modeling suggests a weakened NAM response to increasing temperatures. These illustrate diverging pictures of the NAM response to warming. Here, we examine summer precipitation in the southwestern U.S. related to Last Interglacial insolation forcing. Using a high-resolution climate model, we find that Eemian insolation forcing results in overall wetter conditions throughout most of the southwestern U.S, but significantly drier than present conditions over Arizona. The overall wetter conditions are associated with a northward shift of the anticyclonic circulation aloft and increased moisture in the lower and mid-troposphere during the Eemian. Increased advection of Gulf of Mexico moisture is responsible for increasing precipitation in New Mexico and the northern edges of the NAM region. Drier conditions over Arizona are likely related to reduced local convection associated with reduced vertical moisture transport. These results highlight the spatial complexity of the NAM response to increasing radiative forcing and allow a better understanding of monsoon dynamics and variability in response to a warming climate.

1. Introduction

Precipitation in the southwestern United States is dominated by seasonal monsoonal circulation. The North American Monsoon (NAM) occurs mainly between mid-June to mid-September and provides ~70% of mean annual precipitation to central and northern Mexico and ~35-50% of mean annual precipitation to Arizona and New Mexico in the U.S. (Fig.1a). The NAM shows a strong variability on annual, decadal, and millennial timescales (e.g., Diem et al., 2013; Griffin et al., 2013; Poore et al., 2005) and understanding the response of the monsoonal system to climate change is critical in determining changes in the amount and seasonal distribution of precipitation in this semiarid region of North America. The response of the NAM to increased greenhouse gas forcing and increasing temperature is ambiguous. Previous studies have concluded that global warming was simply delaying the North American monsoon, with no robust changes in total monsoon seasonal rainfall (Cook and Seager, 2013). In contrast, more recent studies (D'Agostino et al., 2019; Pascale et al., 2017; Wang et al., 2020) highlight the possibility of a strong precipitation reduction in the monsoon region in response to future warming, with consequences for regional water resources, agriculture and ecosystems.

These suggested responses of the NAM to current changes in the climate system are distinct from studies providing causes and characteristics of climatic and monsoonal variations over paleo timescales. Insolation is widely regarded as an important control of climate change on long-timescales, particularly in monsoon regions. A strong correlation between summer monsoon intensity and summer insolation has been observed in monsoon records from Asia, South America, and Africa (Cruz et al., 2005; Kutzbach and Liu, 1997; Liu et al., 2006; Wang et al., 2001). Evidence suggests that during insolation maxima, increased summer land-sea temperature contrasts strengthen monsoon systems and shift the summer position of the Intertropical Convergence Zone (ITCZ) further inland (McKay et al., 2011; Montoya et al., 2000). Several records from the U.S. and Mexico exhibit evidence of increased summer convection and precipitation during the warmest periods of the mid-Holocene (Barron et al., 2012; Metcalfe et al., 2015).

To better understand the interplay between rising temperatures and moisture in the NAM region, we chose to focus on the response of the NAM to shifts in orbital forcings during the Last Interglacial (LIG: ~130 to 115ka). The LIG is the most recent period in Earth history when temperatures are believed to have exceeded those of today (Bakker et al., 2013; CAPE members - Anderson, 2006; Kukla et al., 2002; McKay et al., 2011; Turney and Jones, 2010). In particular, the Eemian (~125 ka) is an interval where the Earth was in an orbital configuration that corresponds with insolation maxima and enhanced summer heating of the Northern hemisphere (Berger and Loutr, 1991). The Eemian was warmer than the present day with higher sea level (Bard et al., 1990) and diminished ice sheets (Cuffey and Marshall, 2000). Climate models suggest that the Eemian was a time of increased Northern-Hemisphere temperature and humidity, with a northward–shifted ITCZ, increased summer land-sea temperature contrast, and intensified monsoon convection (Montoya et al., 2000). Numerous studies have focused on the response of polar temperatures to interglacial forcing but less attention has been paid to the regional hydroclimatic changes at the time. These changes are of interest because the response of terrestrial ecosystems to hydroclimate shifts may have been critical to the carbon cycle during the Eemian (Kleinen et al., 2016). For example, favorable redistributions of rainfall into semi-arid regions such as the southwestern U.S. may have acted to increase the terrestrial carbon sink.

Here, we use simulations from a regional climate model (RegCM) under LIG and modern forcings to evaluate changes in the strength, timing, duration, and amount of moisture transported from different sources during the NAM season. The simulated periods are linked with different phases of the interglacial climate system that have been identified in paleodata, namely: the maximum and minimum summer insolation in the northern hemisphere (130 ka and 115ka, respectively) as well as the minimum global ice volume (125 ka). Our simulations intend to complement previous LIG simulations done at lower resolution with a focus on monsoonal dynamics. Among other things, these simulations serve as a reference for new and upcoming proxy records in the southwestern U.S. (e.g., Pigati et al., 2014). Particularly, the data provide background to consider how global carbon cycle dynamics and ecological systems in the southwestern U.S. might have responded to recent periods in Earth history when summer temperatures exceeded those of today (Brown et al., 2014; Elias, 2014; Strickland et al., 2014). Understanding these variations is critical to seasonal supply of water to and habitat changes in the southwestern U.S. under warming conditions. The LIG warming is mostly seasonal and clearly driven by orbital change and should not be used as a direct analogue model to future warming. However, the changes in thermodynamic and dynamic contributions to monsoon precipitation, and in particular changes in moisture fluxes, during the modern and the Eemian can provide important insights into the mechanisms and forcings affecting NAM precipitation.

2. Model Description and Setup

RegCM_4.4.5 (Pal et al., 2007) is a fourth generation, three-dimensional regional climate model, based on the original model developed by Giorgi et al. (1993a; 1993b) with a dynamical core that is adopted from the hydrostatic version of the Pennsylvania State University-National Center for Atmospheric Research Mesoscale Model (MM5) (Grell et al., 1994). It is a primitive-equation, hydrostatic, compressible model with sigma-vertical coordinates (Giorgi et al., 1993a). Improvements in the software code and model physics (e.g., representation of convective schemes, surface physics, atmospheric chemistry and aerosols, ocean-air exchanges) allows an enhanced model performance in monsoonal regions. A full description of RegCM4's basic features and details on the historical evolution of RegCM are given in Giorgi et al. (2012).

RegCM_4.4.5 experiments were performed for North America using a horizontal resolution of 55 km and 18 vertical levels. Lateral boundary conditions are based on data from ERA-Interim reanalysis with a spatial resolution of 1.5°x1.5° (EIN15), while sea-surface temperatures (SSTs) were obtained from the NOAA optimum interpolation (OI) SST analysis (Reynolds et al., 2002). Convective precipitation was computed with the MIT-Emanuel scheme (Emanuel, 1991). It has been shown that RegCM simulations with the cumulus convections scheme and its Emanuel closure assumptions lead to improved simulations of precipitation, temperature and low-level wind patterns in comparison to other cloud and convection parameterizations (Pal et al., 2007; Sinha et al., 2019; Velikou and Tolika, 2017). In particular, RegCM has been widely applied in limited-domain, seasonal forecasts and used to simulate climate in high-precipitation monsoonal regions and around the globe (e.g., Diro et al., 2012; Fuentes-Franco et al., 2014; Insel et al., 2009; Sylla et al., 2010). The goal of this study is to quantify the impact of orbital parameters on North American Monsoon dynamics. Our model domain ranges from 128° W to 82° W along the southern domain margin at ~10° N and from 150° W to 60° W along the northern domain margin at ~60° N (Fig. 1). The domain includes parts of the eastern Pacific and the Gulf of Mexico to accurately simulate climate pattern and source regions over oceanic areas. We designed 4 experiments to account for different orbital parameter configurations during the LIG and changing greenhouse gas concentrations (Table 1). In particular, we simulated interglacial time slices to capture the obliquity minimum and maximum (MinObliquity = 115 ka, MaxObliquity = 130 ka; (Berger and Loutr, 1991)), respectively, and a third time slice that falls between these two (Eemian = 125ka). Simulations were 21 years in length and results are based on the last 20 years of the simulations. While the length of spin-up time is dependent on model domain, season, and circulation intensity, previous studies have shown that regional climate models are usually representing a dynamic equilibrium after just a few months (Zhong et al., 2007)

Small discrepancies with observations may arise due to the experimental design, which include the use of present-day vegetation and polar ice sheets as well as consistent sea surface temperatures. Modern boundary conditions for geography, ice sheets, and vegetation follow previous studies simulating temperature and precipitation responses in the United States to interglacial warm periods (e.g., Diffenbaugh et al., 2006; Otto-Bliesner et al., 2013). Moreover, Diffenbaugh et al. (2006) indicated that general precipitation patterns over the U.S. do not change in response to sea surface temperatures changes in orbital-driven warm periods. They observed that at least some localities showed greater agreement with the proxy record in experiments without changes in SSTs as compared to a more complete ocean treatment. While the regional simulation by Diffenbaugh et al. (2006) indicate a spring and summer dry bias over parts of the southwestern U.S., the overall precipitation pattern is well represented.

3. Results

3.1. Model Validation

A comparison between simulated and observed data indicates that RegCM_4.4.5 performs well in capturing the general climatology in the western part of North America (Fig. 1). The model performance for modern precipitation is assessed by using independent precipitation observations from the Global Precipitation Climatology Centre (GPCC) data base (Schneider et al., 2011). Figure 1a shows the NAM expressed as percent of annual precipitation that falls in July to September (JAS). The model captures the spatial distribution of monsoon precipitation across the western United States and Mexico, including regions of maximum precipitation along the west coast of Mexico (Fig 1b). Moreover, the model is consistent with the climatological monthly precipitation averaged over the main region of the NAM. The region is semiarid with a single precipitation maximum evident in the summer months with averaged maximum precipitation of around 3.5 mm/day (Fig 1c). The model captures the July precipitation, but slightly overestimates precipitation in August and September. We attribute this discrepancy to the model resolution and a slight summer warm bias over the southwestern U.S (Figure S1a, b) that likely overestimate the moisture component that is transported from the oceans to the land, resulting in higher precipitation rates. A model data comparison indicates a wet bias over the core of the NAM region in southern Mexico, and a dry bias along the western continental Mexican coast (Figure S1c, d). However, the main spatial and temporal patterns of monsoonal precipitation are well established in our model simulations.

3.2. Insolation and Temperature

The changes in the amount of insolation received by the Earth during LIG result from changes in the astronomical configuration. During MaxObliquity (130 ka) and in the Eemian (125 ka), our study area received more insolation in spring and summer compared to modern (Fig. 2a, b). Focusing on the NAM area, the difference in incoming shortwave flux at the top of the atmosphere between the warm LIG periods and present is approximately 45 Wm^{-2} in June and -25 Wm^{-2} in December. However, MaxObliquity indicates stronger insolation in particular from late February to July, while the Eemian is characterized by stronger insolation from late April to September (Fig. 2a). In contrast, MinObliquity (115 ka) indicates the opposite pattern in insolation with below modern values in spring and summer and above modern values during the fall and winter. The magnitude of changes between MinObliquity and modern is overall smaller with around -20 Wm^{-2} in June and 20 Wm^{-2} in December.

In response to increased insolation in northern hemisphere spring and summer during 130 ka and 125 ka, simulated surface temperatures are generally higher during those periods compared to the modern over the majority of the western and southwestern U.S. Positive temperature anomalies averaged over the NAM region are observed in April, May and June during the early LIG (Fig. 2c, d). Temperature anomalies indicate strong spatial variability with up to 2°C higher temperatures in New Mexico and Arizona, but similar to present temperatures in central and western Mexico (Fig. 3). Warming is stronger and occurs earlier at 130 ka in comparison to 125 ka. In July and August, surface temperatures are cooler in most parts of the monsoon region with regional temperature differences of up to -1.5° C compared to present. Most cooling is observed along the west coast of Mexico and Baja California. This is opposite to the expected direct radiative effect, and might be due to increased cloudiness, evapotranspiration, and precipitation (Fig. 2e-k). During MinObliquity, surface temperatures in the southwestern U.S. are generally colder than present throughout the entire spring and summer, corresponding to reduced insolation at that time (Fig. 2, 3).

3.3. North American Monsoon Pattern (Modern versus Eemian)

Simulated precipitation is the sum of large-scale precipitation related to cyclones or frontal systems, and convective precipitation associated with local surface heating and vertical air movement. The NAM system is associated with a dramatic increase in summer precipitation. Averaged over the entire monsoon region, precipitation magnitudes over land reach a maximum around 130 mm/month in July and August (Fig. 2e). Modern precipitation is spatially very variable with the highest precipitation rates in Mexico and significant less precipitation across the southwestern U.S. (Fig. 4a).

Precipitation associated with the NAM system can be related to a thermodynamic component (linked to atmospheric moisture content changes) and a dynamic component (linked to atmospheric circulation changes). Seasonal warming results in higher atmospheric moisture content. The onset of the monsoon season in July is characterized by a significant increase in relative humidity along the flanks of the Mexican Plateau and Arizona and New Mexico (Fig. 5a-b, d-e). High surface specific humidity on either side of the Mexican Plateau is consistent with the spatial gradient of NAM precipitation with higher precipitation magnitudes in Mexico and lower precipitation magnitudes in the southwestern U.S. (Fig. 7a). Vertical moisture advection is evident in strong upward motion (Fig. 6a, c), in particular along the western flank of the Mexican plateau. Warm air over land is more buoyant and destabilizes the atmospheric column directly above. As a result, atmospheric convection is dominant and most of the monsoonal precipitation is convective in origin (~80-90%, Fig. 2g).

To identify the origin of the low-level moistening through horizontal moisture advection, vertically integrated and zonal moisture fluxes, monthly mean winds, and the moisture flux convergence are examined. The integrated mass-weighted zonal moisture flux increases significantly at the onset of the monsoon season (Fig. 5g, h). Strong winds transport water vapor from the Gulf of Mexico (GoM) into the eastern part of the NAM region. The strongest flux onto the terrestrial NAM region occurs at low levels by southeasterly winds (Fig. 7 a, b).

Moisture in Arizona appears to originate from the Gulf of California (GoC) and the eastern tropical Pacific. Strong northwesterly winds associated with the large-scale circulation in the east Pacific anticyclone occur west of Baja California. Along the west coast, the low-level flow is primarily parallel to the continent with little influx of moisture (Fig. 7a). The elevated topography of the Mexican Plateau blocks and deflects low-level winds and divides the water vapor sources with a moist tongue extending up the Gulf of California on the west side and increased amounts of water vapor extending from the Gulf of Mexico on the east side (Fig. 7b). Moisture divergence at 700 hPa is localized over the Gulf of California and in the southeastern region of the GoM, suggesting that these oceanic regions are the primary sources for NAM moisture (Fig. 7c).

The large-scale, 500-hPa and 200-hPa wind fields show large anticyclonic rotation over the southwestern U.S. (Fig. S2) and steer moisture transport at lower levels predominantly from the Gulf of Mexico.

During the LIG, the overall precipitation pattern and length of the monsoon season is similar to today with a strong summer monsoon and dry winter months. However, during the Eemian (125 ka), precipitation over the NAM region slightly increases in spring, and is considerably higher in July and August in comparison to the present (Fig. 2e, f). Averaged over the entire monsoon region, monthly precipitation magnitudes were about 24 mm higher in July and 14 mm higher in August.

The changes in monsoonal precipitation during the Eemian were not uniform, but indicate strong spatial variability. JJA precipitation increased by up to 60 % in the eastern half of the monsoon region, but decreased by 40 % over Arizona in the northwestern part of the NAM region (Fig. 4c). Increased Eemian precipitation can be related to an increase in moisture due to an overall warmer atmosphere. Simulated air temperature over the GoM is slightly warmer in the Eemian compared to modern (Fig. 3). The warmer temperatures over the GoM and along a narrow corridor from the east coast of Mexico into New Mexico and the northern part of Arizona provides a basis for increased saturation vapor pressure. It results in more moisture available in the atmosphere to condense into precipitation, favoring more intense cloud fraction, humidity, and monsoonal precipitation (Fig. 2, 5). However, the vertical velocity across the NAM region is less (Fig. 6b, d) and convective precipitation changes very little (Fig. 2g), so most of the additional precipitation must be related to large-scale phenomena.

Stronger horizontal moisture transport into the core and eastern part of the monsoon region during the Eemian is evident (Fig. 7d, e). Surface winds increase around 15 % over the Gulf of Mexico and the Gulf of California (Fig S2, S3), transporting more moisture into north-central Mexico, New Mexico and California and leading to increased evapotranspiration (2j, k). Increased wind speeds and moisture transport is accompanied by a northward shift of the anticyclonic wind pattern (Fig. S2).

Although most of the monsoon region indicates an increase in precipitation during the Eemian, Arizona shows a pronounced drying (Fig. 4c). Lower precipitation in the western part of the monsoon region is not immediately evident in other moisture quantities. Specific and relative humidity during the Eemian are high in the region. Horizontal moisture transport is evident in 35% stronger surface winds over Arizona and an increase in mass-weighted integrated zonal moisture flux over the GoC (Fig 5i). However, the vertical moisture flux is reduced (Fig. 6). Most of the precipitation over the NAM region is convective in origin, but the climatological conditions that promote convection differ between regions (Adams and Comrie, 1997; Douglas et al., 1993). In the western NAM region, convection depends essentially on the presence of lower-troposphere moisture with intense insolation and elevated topography (Adams and Souza, 2009). Simulated air temperature over the eastern subtropical Pacific and over the Gulf of California (GoC) is colder in JJA which is in agreement with suggested Eemian cooling in the subtropical Pacific based on Mg/Ca observational data (Leduc et al., 2010). Lower air temperatures around Baja California may weaken velocity potential and convection in the western part of the NAM region. Examination of the vertical structure during the Eemian indicates less vertical air motion (fig. 6), less moisture flux divergence (Fig. 7) and an upper-tropospheric (200-hPa) divergence (not shown) that coincides with reduced mid-tropospheric vertical motion, reduced convection, and reduced monsoon rainfall in Arizona. Higher surface winds over Arizona may result in moving water vapor out of the area to the east. Surface winds are from the southwest but shift from a more meridional to a more zonal direction (i.e., a stronger westerly component, Fig. S3). This could explain an increase in California precipitation, while Arizona experiences drier conditions.

3.4 Temporal Monsoon Variability during LIG

Our model simulates positive temperature anomalies in early summer across the western U.S. in response to the dominant orbital forcing mechanism that modifies the incoming solar radiation during the early stages of the LIG (130 ka and 125 ka). Despite similar orbital forcing configurations during the warm phase of the LIG, the monsoonal climate during 130ka and 125ka is quite different.

Obliquity is largest at 130 ka and peaked earlier than precession during the LIG (Crowley and Kim, 1994). The obliquity affects seasonal contrast and results in stronger monthly temperature deviations at 130 ka than 125 ka in comparison to modern simulations (Fig. 2). However, simulations show that the NAM response is dominated by precession. Positive temperature anomalies averaged over the NAM region are significantly higher in spring at 130 ka than at 125 ka. While July temperature anomalies differ spatially under Eemian conditions, the average temperature across the NAM region is similar to MaxObliquity. This is consistent with a shift in perihelion from earliest May at 130 ka to late July at 125 ka and associated impacts on Northern Hemisphere insolation (Otto-Bliesner et al., 2013).

The timing of perihelion increased the seasonal insolation and temperature contrast; an effect that was amplified by the highly eccentric orbit. The overall cooler temperatures in the late summer months during 130 ka taper the monsoonal response. Averaged over the entire NAM region, MaxObliquity indicates a larger positive precipitation anomaly in May, when insolation is the highest, but experiences an overall similar monsoon as present, with slightly higher precipitation magnitudes in June and July (Fig. 2). JJA spatial pattern indicate a maximum increase in precipitation of around 30-40 % in the core region of the NAM, while the eastern and western coast of Mexico indicate a modest decrease around 10-20 % or no significant change in precipitation in comparison to modern (Fig. 4d). Arizona experiences a similar pattern to the Eemian with a precipitation decrease up to 35 %. Overall, MaxObliquity indicates a similar precipitation pattern as the Eemian, with moisture flux changes representing the same spatial distribution, but smaller changes in magnitudes (Fig. S4)

While we are mainly focusing on the warm periods of the early LIG, we want to present a short summary of climate changes related to MinObliquity. Eccentricity is large throughout the entire LIG. With minimum obliquity and perihelion in January, seasonal contrasts at 115 ka are moderate. In response to lower insolation and lower temperature in spring and summer, the NAM region is slightly dryer with precipitation about 5 to 10 % lower than modern. The decrease in total precipitation is mostly due to a slight decrease in convection and associated less intense storm events throughout the summer. MinObliquity is characterized by a strong reduction in moisture at the lower and middle troposphere. The extent and magnitude of drying is similar to the spatial pattern observed for increased humidity in the Eemian. Maximum decrease in surface moisture is observed in the NAMeast region and north of the core monsoon (Fig. S4), while moisture in the middle troposphere decreases uniformly, but only at small magnitudes. The upper level anticyclone weakens and shifts southeast (Fig. S2).

4. Discussion

Overall, our simulations suggest a temporally and spatially diverse response to insolation changes in the North American Monsoon region. We attribute the difference in the timing and magnitude of maximum insolation and temperature changes to changes in obliquity and precession. Previous studies (e.g., Bakker et al., 2013; Otto-Bliesner et al., 2013) have shown that the radiative forcing provided by the changes in the three major GHGs is small (< 0.2 W m^{-2}) compared to the forcing provided by the insolation changes. Our simulated June and July temperatures are consistent with results from earlier model inter-comparison studies that show robust Northern Hemisphere July temperature evolution characterized by a maximum between 130 – 125 ka with temperatures 0.3 to 5.3 K above modern (Bakker et al., 2013; Lunt et al., 2013). Proxy datasets of quantitative estimates of mean annual surface temperatures only include a limited number of terrestrial sites in the U.S. However, intact Eemian wood samples have been recovered from sediments of the Ziegler Reservoir in Snowmass Colorado (Pigati et al., 2014). A unit corresponding to MIS 5e has been dated to between ~126 and 120 ka with mean July temperature reconstruction that have been similar to or slightly warmer than they are today (Elias, 2014). Interestingly, the core region of the NAM region, including northwestern Mexico and southwestern Arizona, indicates cooling in July and August. This pattern is consistent with previous model results that show continental cooling at subtropical northern latitudes associated with the core regions of other monsoon systems such as Asian and African systems (Otto-Bliesner et al., 2013). Previous studies have attributed cooler summer temperature during the early LIG to enhanced summer monsoons and cloud feedbacks. A comparison between TOA and surface insolation (Fig. 2a, b) suggests atmospheric processes enhance reflection and/or scattering of incoming solar radiation. Increased atmospheric water vapor during the Eemian (evident in the cloud fraction, total columnar liquid water content, and integrated moisture fluxes (Fig 2h, I; Fig. 5)) may contribute to the cooling pattern.

Our model indicates northward movement of the mid-level anticyclone and warming over the Gulf of Mexico that facilitates stronger moisture transport into the eastern NAM region. An intensification of precipitation over most of the southwestern U.S. during the Eemian is consistent with previous studies that suggest a more intense NAM in response to increased Northern Hemisphere insolation (Asmerom et al., 2007; Barron et al., 2012; Metcalfe et al., 2015). A recent study by Scussolini et al. (2019) compares simulated hydroclimates in LIG model experiments with proxy data and explores the limitations of data-model comparisons. In very good agreement with our simulation, Scussolini's model ensemble shows higher average precipitation of the NAM during the early LIG by about 34%. However, the models used in that study indicate considerable variability with at least one model suggesting a noticeable decrease in monsoonal precipitation during the LIG (Scussolini et al., 2019). Very few terrestrial LIG proxies exist in the southwestern U.S. and none of them unambiguously project seasonal precipitation anomalies. Multiproxy data from wetland records in Colorado (Miller et al., 2014) and pollen proxies from ancient lakes in California (Bradbury, 1997; Ku et al., 1998; Menking et al., 1997; Reheis et al., 2012) suggest overall wetter conditions during the early LIG, but it is not clear whether these anomalies are related to summer or winter precipitation.

Our model predicts an increase in monsoonal precipitation over most parts of the southwestern U.S., but also distinctively drier conditions over the northwest corner of the core monsoonal area in Arizona. We are not aware of datasets that can verify or refuse the idea of regional drying in parts of the NAM during the Eemian. Paleoclimate model simulations are usually conducted with lower-resolution general circulation models that provide large-scale information, but do not resolve small-scale regional variations. However, the modeled spatial variability in monsoonal precipitation is consistent with the dual nature of the modern monsoon, where anomalously wet periods in New Mexico do correspond to low precipitation periods in Arizona or vice versa, supporting the evidence of different moisture sources and paths for the two regions (Comrie and Glenn, 1998).

The climate of the Eemian is closely related to the orbital forcing configurations that result in a pronounced seasonal cycle with warmer summers and colder winters. Current and future climate change is associated with greenhouse gas radiative forcing that will most likely result in uniformly warm conditions throughout the year. While the difference in forcing factors might limit our expectations of a direct comparison between the two warming scenarios, positive temperature anomalies and associated patterns in hydroclimate have been proposed in future climate projections (D'Agostino et al., 2019; Wang et al., 2020). There is observational evidence to suggest that monsoon precipitation is becoming more extreme in the Southwest and northwestern Mexico with increasing surface temperatures (Anderson et al., 2010; Chang et al., 2015; Luong et al., 2017). An overall stronger monsoon can be explained by strong feedbacks between summer insolation, evapotranspiration, convection, and cloudiness. However, summertime convective activity in the southwestern U.S. is spatially variable and results from complex interactions between atmospheric circulation features and the complex topography (Adams and Souza, 2009). Drier conditions in Arizona may reflect local topographic effects that are critical to the distribution of convective activity. Adams and Comrie (1997) discussed the formation of the NAM in response to temperature contrasts between seasonally warm low land surfaces and elevated areas together with atmospheric moisture supply from nearby maritime source. In the modern context, the thermal contrast in the Gulf of California facilitates the formation of moisture-laden air masses that move northward toward a region of low pressure centered over Arizona (Pascale and Bordoni, 2016; Wu et al., 2009). Our simulations show a decrease in temperature in the low-lying regions of Arizona, which reduces the thermal low and reduces convective precipitation (Fig. 4, 6). Our results are in agreement with Pascal et al. (2017) who highlights the possibility of a strong precipitation reduction in the northwestern edge of the monsoon region in response to increased atmospheric stability and weakened convection.

It is important to note that most of the NAM literature has a strong geographical bias toward the state of Arizona, but differences in precipitation response between the eastern and western NAM regions are very apparent in our model output as well as modern observations (Comrie and Glenn, 1998). Our model simulations suggest that in an orbital forcing-induced warmer climate, NAM regions that are dominated by local convection and vertical moisture advection experience drier conditions, while regions dominated by horizontal, regional moisture fluxes may experience wetter conditions. Our findings are consistent with present-day analysis from the Climate Prediction Center and individual Cooperative Observer Program (COOP) stations with long-term records of precipitation in the southwestern U.S. that indicate a significant increase in mean precipitation in New Mexico, but a decrease in mean monsoon precipitation over Arizona in recent decades (Luong et al., 2017).

The precipitation response to increased solar radiation and associated warming is complex. The NAM region does not experience a uniform response to changing climate conditions. A more detailed analysis with high-resolution models (<25 to 10km resolution) is necessary to account for a thorough examination of the Gulf of California response to insolation changes. We may not accurately resolve the summertime low-level flow along the Gulf of California which may impact precipitation estimates in the southwestern US. However, our model results are in good agreement with previous studies trying to unravel the NAM history in response to warmer interglacial periods as well as modern observations in a warming climate.

Acknowledgements:

This study was supported by the National Science Foundation grant NSF EAR 1502772. The work was completed in part with resources and assistance provided by the University of Chicago

Research Computing Center. We thank two anonymous reviewers for constructive comments on the manuscript.

Data Availability:

The data (NetCDF files from climate simulations) that support the findings of this study are available from the corresponding author upon reasonable request.

Figures:

Figure 1: Measured and simulated monsoonal precipitation across North America. (a) Precipitation (in percent of annual precipitation) during the peak NAM season (July, August, September = JAS) based on observations from the Global Precipitation Climatology Centre (GPCC) database from 1981 to 2010. (b) RegCM4 simulated 20-year mean JAS precipitation. Red box highlights the main NAM monsoon region, green box indicates Arizona 'dry' region (see text for explanation). (c) Monthly precipitation flux of observed and simulated precipitation over the monsoon region.

Figure 2: Simulated forcing factors and climate parameters averaged over the North American Monsoon region for 4 cases: modern (black line), 115 ka (blue line), 125 ka (green line), and 130 ka (red line). (a) Incoming solar radiation at the top of the atmosphere indicates higher incoming shortwave flux during the early LIG. (b) Surface net shortwave flux highlights cloud feedbacks during the summer months. (c) and (d) Surface temperature and highlighted differences in temperature between case studies and modern. (e) and (f) Total precipitation and difference in precipitation between case studies and modern. (g) Convective precipitation. Large differences in total precipitation, but small differences in convective precipitation during the Eemian highlights the impact of additional large-scale transport of moisture into the study area. (h) Total cloud fraction (i) Total liquid water content. (j) and (k) Total evapotranspiration flux and difference in evapotranspiration between case studies and modern. Averaged over the monsoon region, climate parameters suggest an increase in atmospheric moisture during the early LIG.

Figure 3: Simulated temperature differences between LIG and modern from May to August. Top row: Difference in temperature between MinObliquity and modern. Middle row: Temperature differences between Eemian and modern. Bottom row: Temperature difference between MaxObliquity and modern. The monthly maps indicate surface temperature with fixed ocean temperature. Notice lower temperatures in July and August in the NAM region. The right column shows near surface air temperature differences averaged over June, July, August. Although sea

surface temperatures have been held constant in the model, the air temperature increases over the Gulf of Mexico and decreases over the Gulf of California during 125 ka and 130 ka.

Figure 4: Simulated precipitation differences (in percentage) between LIG and modern for June, July, August (JJA). (a) Simulated summer precipitation (in mm/day) over the U.S. (b-d) Difference in precipitation between (b) MinObliquity and modern; (c) Eemian and modern; (d) MaxObliquity and modern. Notice duality pattern between Arizona and eastern monsoon region.

Figure 5: Relative humidity (RH) and mass-weighted integrated moisture flux across the NAM region. (a, b) Increased modern RH from June to July across Arizona and New Mexico at around 32°N at the onset of the North American monsoon season. (c) RH along the same profile during Eemian July. (d-f) Same as (a-c) but for a profile across the Mexican Plateau at around 26°N. (g, h) Distribution of integrated mass-weighted zonal moisture flux at the onset of the North American monsoon season. Modern simulations indicate increase in moisture from June to July over the key source regions of the NAM. (i) Eemian simulation indicates stronger mass-weighted integrated moisture flux in comparison to modern.

Fig. 6: Vertical velocity (omega) across the NAM region in July. Negative values indicate upward air component. (a) Vertical motion across Arizona and New Mexico at around 32°N at the onset of the North American monsoon season. (b) Reduced vertical motion during the Eemian. (c-d) Same as (a-b) but for a profile across the Mexican Plateau at around 26°N. Strong uplift is evident along the western flank of the Mexican Plateau. Reduced motion during the Eemian.

Figure 7: Horizontal moisture flux quantities at different heights averaged over June, July, August. (a) Surface specific humidity (colored) and winds in modern simulation shows distinct moisture sources for Arizona and New Mexico. (b) Modern zonal moisture at 850 hPa. Positive values indicate westerly moisture flux, negative values indicate easterly moisture flux. (c) Modern velocity potential (colored) and moisture flux divergence at 700 hPa. (d - f) Differences between Eemian and modern moisture flux in comparison to (a-c). Positive values indicate higher moisture (flux) during Eemian, negative values indicate less moisture (flux).

Table 1: Forcings and boundary conditions used in RegCM simulations.

Supplement Figure S1: Comparison of modeled data versus observations for summer (JJA) temperature and precipitation. (a) Observed summer precipitation, based on CRU data (1981-2010). (b) RegCM modeled summer temperature. (c) Observed summer precipitation, based on precipitation time series from the Global Historical Climatology Network (GHCN) database (1981-2010). (d) RegCM modeled summer precipitation.

Supplement Figure S2: Wind patterns averaged over JJA in the Modern and during the Eemian. (a-c) Modern winds at the surface, 500-hPa, and 200-hPa. The model realistically simulates the anticyclonic patterns at mid- and high-levels. (d-e) Vectors are showing difference in wind magnitude under Eemian and modern conditions. Vector colors indicate magnitude, positive and negative signs are related to the change in physical direction of winds.

Supplement Figure S3: Surface moisture (white-blue) and surface winds during JJA. (a) Map view shows distinct moisture sources for Arizona and New Mexico. (b) Changes in wind speed (wdsp) and wind direction (wdd) under modern and Eemian conditions for different regions associated with the NAM.

Supplement Figure S4: Comparison of moisture flux between modern, MaxObliquity and MinObliquity. Top row: modern simulations. Middle row: Difference between Max Obliquity (130 ka) and modern. Bottom Row: Difference between MinObliquity (115 ka) and modern.

Bibliography:

Adams, D.K. and Comrie, A.C., 1997. The North American Monsoon. Bulletin of the American Meteorological Society, 78(10): 2197-2213.

Adams, D.K. and Souza, E.P., 2009. CAPE and Convective Events in the Southwest during the North American Monsoon. Monthly Weather Review, 137(1): 83-98.

Anderson, B.T., Wang, J., Salvucci, G., Gopal, S. and Islam, S., 2010. Observed Trends in Summertime Precipitation over the Southwestern United States. Journal of Climate, 23(7): 1937-1944.

Asmerom, Y., Polyak, V., Burns, S. and Rassmussen, J., 2007. Solar forcing of Holocene climate: New insights from a speleothem record, southwestern United States. Geology, 35(1): 1.

Bakker, P., Stone, E.J., Charbit, S., Groeger, M., Krebs-Kanzow, U., Ritz, S.P., Varma, V., Khon, S., Lunt, D.J., Mikolajewicz, U., Prange, M., Renssen, H., Schneider, B. and Schulz, M., 2013. Last interglacial temperature evolution - a model inter-comparison. Climate of the Past Discussions, 8: 4663-4699.

Balaguru, K., Foltz, G.R. and Leung, L.R., 2018. I^{n}creasing Magnitude of Hurricane Rapid Intensification in the Central and Eastern Tropical Atlantic. Geophysical Research Letter, 45(9): 4238-4247.

Bard, E., Hamelin, B. and Fairbanks, R.G., 1990. U-Th ages obtained by mass spectrometry in corals from Barbados: sea level during the past 130,000 years. Nature, 346: 456- 458.

Barron, J.A., Metcalfe, S.E. and Addison, J.A., 2012. Response of the North American monsoon to regional changes in ocean surface temperature. Paleoceanography, 27.

Bathia, K., Vecchi, G.A., Knutson, T.R., Murakami, H., Kossin, J., Dixon, K.W. and Whitlock, C.E., 2019. Recent increases in tropical cyclone intensification rates. Nature Communications.

Berger, A. and Loutr, A.F., 1991. Insolation Values for the Climate of the Last 10 Million Years. Quaternary Science Reviews, 10: 297 - 317.

Bradbury, J.P., 1997. A Diatom Record of Climate and Hydrology for the past 200 ka from Owens Lake, California with Comparison to Other Great Basin Records. Quaternary Science Reviews, 16: 203-219.

Brown, P.M., Nash, S.E. and Kline, D., 2014. Identification and dendrochronology of wood found at the Ziegler Reservoir fossil site, Colorado, USA. Quaternary Research, 82(3): 575-579.

CAPE members - Anderson, P., Bennike, O., Bigelow, N., Brigham-Grette, J., Divall, M., Edwards, M., Frechette, 2006. Last Interglacial Arctic warmth confirms polar amplification of climate change. Quaternary Science Reviews, 25(13-14): 1383-1400.

Chang, H.I., Castro, C.L., Carrillo, C.M. and Dominguez, F., 2015. The more extreme nature of U.S. warm season climate in the recent observational record and two “well‐performing” dynamically downscaled CMIP3 models. Journal of Geophysical Research: Atmospheres, 120(16): 8244-8263.

Comrie, A.C. and Glenn, E.C., 1998. Principle components-based regionalization of precipitation regimes across the southwest United States and northern Mexico, with an application to monsoon precipitation variability. Climate Research, 10: 201 - 215.

Cook, B.I. and Seager, R., 2013. The response of the North American Monsoon to increased greenhouse gas forcing. 118(4): 1690-1699.

Corbosiero, K.L., Dickinson, M.J. and Bosart, L.F., 2009. The Contribution of Eastern North Pacific Tropical Cyclones to the Rainfall Climatology of the Southwest United States. Monthly Weather Review, 137(8): 2415-2435.

Crowley, T.J. and Kim, K.-Y., 1994. Milankovitch Forcing of the Last Interglacial Sea Level. Science, 265(5178): 1566-1568.

Cruz, F.W., Jr, Burns, S., J., Karmann, I., Sharp, W.D., Vuille, M., Cardoso, A.O., Ferrari, J.A., Silva Dias, P.L. and Vlana Jr, O., 2005. Insolation-driven changes in atmospheric circulation over the past 116,000 years in subtropical Brazil. Nature, 434: 63 - 66.

Cuffey, K.M. and Marshall, S.J., 2000. Substantial contribution to sea-level rise during the last interglacial from the Greenland ice sheet. Nature, 404: 591 - 594.

D'Agostino, R., Bader, J., Bordoni, S., Ferreira, D. and Jungclaus, J., 2019. Northern Hemisphere Monsoon Response to Mid-Holocene Orbital Forcing and Greenhouse Gas-induced Global Warming. Geophysical Research Letter.

Diem, J.E., Brown, D.P. and McCann, J., 2013. Multi-decadal changes in the North American monsoon anticyclone. International Journal of Climatology, 33(9): 2274-2279.

Diffenbaugh, N.S., Ashfaq, M., Shuman, B., Williams, J.W. and Bartlein, P.J., 2006. Summer aridity in the United States: Response to mid-Holocene changes in insolation and sea surface temperature. Geophysical Research Letters, 33(22).

Diro, G.T., Rauscher, S.A., Giorgi, F. and Tomkins, A.M., 2012. Sensitivity of seasonal climate and diurnal precipitation over Central America to land and sea surface schemes in RegCM4. Climate Research 2: 31-48.

Douglas, M.W., Maddox, R.A., Howard, K. and Reyes, S., 1993. The Mexican Monsoon. Journal of Climate, 6: 1665-1667.

Elias, S.A., 2014. Environmental interpretation of fossil insect assemblages from MIS 5 at Ziegler Reservoir, Snowmass Village, Colorado. Quaternary Research, 82(3): 592-603.
Emanuel, K.A., 1991. A Scheme for Representing Cumulus Convection in Large-Scale Models. Journal of the Atmospheric Sciences, 48(21): 2313-2329.
Englehart, P.J. and Douglas, A.V., 2001. The role of eastern North Pacific tropical storms in the rainfall climatology of western Mexico. International Journal of Climatology, 21(11): 1357-1370.
Frappier, A., Knutson, T., Liu, K.-B. and Emanuel, K., 2007. Perspective: coordinating paleoclimate research on
tropical cyclones with hurricane-climate theory
and modelling. Tellus, 59A: 529-537.
Fuentes-Franco, R., Coppola, E., Giorgi, F., Graef, F. and Pavia, E.G., 2014. Assessment of RegCM4 simulated inter-annual variability and daily-scale statistics of temperature and precipitation over Mexico. Climate Dynamics, 42: 629-647.
Giorgi, F., Coppola, E., Solmon, F., Mariotti, L., Sylla, M., Bi, X., Elguindi, N., Diro, G., Nair, V., Giuliani, G., Turuncoglu, U., Cozzini, S., Güttler, I., O'Brien, T., Tawfik, A., Shalaby, A., Zakey, A., Steiner, A., Stordal, F., Sloan, L. and Brankovic, C., 2012. RegCM4: model description and preliminary tests over multiple CORDEX domains. Climate Research, 52: 7-29.
Giorgi, F., Marinucci, M.R. and Bates, G.T., 1993a. Development of a Second-Generation Regional Climate Model (RegCM2). Part I: Boundary-Layer and Radiative Transfer Processes. Monthly Weather Review, 121(10): 2794-2813.
Giorgi, F., Marinucci, M.R., Bates, G.T. and De Canio, G., 1993b. Development of a Second-Generation Regional Climate Model (RegCM2). Part II: Convective Processes and Assimilation of Lateral Boundary Conditions. Monthly Weather Review, 121(10): 2814-2832.
Grell, G.A., Dudhia, J. and Stauffer, D.R., 1994. A Description of the Fifth-Generation PennState/NCAR Mesoscale Model (MM5). NCAR technical report, TN-398+STR: p 121.
Griffin, D., Woodhouse, C.A., Meko, D.M., Stahle, D.W., Faulstich, H.L., Carrillo, C., Touchan, R., Castro, C.L. and Leavitt, S.W., 2013. North American monsoon precipitation reconstructed from tree-ring latewood. Geophysical Research Letters, 40(5): 954-958.
Higgins, R.W., Yao, Y. and X.L, W., 1997. Influence of the North American Monsoon System on the U.S. Summer Precipitation Regime. Journal of Climate, 10: 2600 - 2622.
Holland, G. and Bruyère, C.L., 2014. Recent intense hurricane response to global climate change. Climate Dynamics, 42: 617-627.
Insel, N., Poulsen, C. and Ehlers, T., 2009. Influence of the Andes Mountains on South American moisture transport, convection, and precipitation. Climate Dynamics, 35: 1477-1492.
Kleinen, T., Brovkin, V. and Munhoven, G., 2016. Modelled interglacial carbon cycle dynamics during the Holocene, the Eemian and Marine Isotope Stage (MIS) 11. Climate of the Past, 12(12): 2145-2160.
Ku, T.-L., Luo, S., Lowenstein, T.K., Li, J. and Spencer, R., 1998. U-Series Chronology of Lacustrine Deposits in Death Valley, California. Quaternary Research, pp. 261-275.
Kukla, G.J., Bender, M.L., de Beaulieu, J.-L., Bond, G. and Broecker, W.S., 2002. Last Interglacial Climates. Quaternary Research, 58: 2-13.
Kutzbach, J.E. and Liu, Z., 1997. Response of the African Monsoon to Orbital Forcing and Ocean Feedbacks in the Middle Holocene. Science, 278(5337): 440-443.
Leduc, G., Schneider, R., Kim, J.H. and Lohmann, G., 2010. Holocene and Eemian sea surface temperature trends as revealed by alkenone and Mg/Ca paleothermometry. Quaternary Science Reviews, 29(7-8): 989-1004.

Liu, X., Liu, Z., Kutzbach, J.E., Clemens, S.C. and Prell, W.L., 2006. Hemispheric Insolation Forcing of he Indian Ocean and Asian Monsoon: Local versus Remote Impacts. American Meteorological Society, 19: 6195 - 6208.

Lunt, D.J., Abe-Ouchi, A., Bakker, P., Berger, A., Braconnot, P., Charbit, P., Fischer, N., Herold, N., Jungclaus, J.H., Khon, V.C., Krebs-Kanzow, U., Langebroek, P.M., Lohmann, G., Nisancioglu, K.H., Otto-Bliesner, B.L., Park, W., Pfeiffer, M., Phipps, S.J., Prange, M., Rachmayani, R., Renssen, H., Rosenbloom, N., Schneider, B., Stone, E.J., Takahashi, K., Wei, W., Yin, Q. and Zhang, Z.S., 2013. A multi-model assessment of last interglacial temperatures. Climate of the Past, pp. 699-717.

Luong, T.M., Castro, C.L., Chang, H.-I., Lahmers, T., Adams, D.K. and Ochoa-Moya, C.A., 2017. The More Extreme Nature of North American Monsoon Precipitation in the Southwestern United States as Revealed by a Historical Climatology of Simulated Severe Weather Events. Journal of Applied Meteorology and Climatology, 56(9): 2509-2529.

McKay, N.P., Overpeck, J.T. and Otto-Bliesner, B.L., 2011. The role of ocean thermal expansion in Last Interglacial sea level rise. Geophysical Research Letters, 38(14): n/a-n/a.

Menking, K.M., Bischoff, J.L., Fitzpatrick, J.A., Burdette, J.W. and Rye, R.O., 1997. Oscillations since 155,000 yr BP at Owens Lake, California, Reflected in Abundance and Stable Isotope Composition of Sediment Carbonate. Quaternary Research, pp. 58-68.

Metcalfe, S.E., Barron, J.A. and Davies, S.J., 2015. The Holocene history of the North American Monsoon: ‘known knowns’ and ‘known unknowns’ in understanding its spatial and temporal complexity. 120: 1-27.

Miller, D.M., Miller, I., M. and Jackson, S.T., 2014. Biogeography of Pleistocene conifer species from the Ziegler Reservoir fossil site, Snowmass Village, Colorado. Quaternary Research, 82: 567-574.

Montoya, M., von Storch, H. and Crowley, T.J., 2000. Climate Simulation for 125 kyr BP with a Coupled Ocean-Atmosphere General Circulation Model. Journal of Climate, 13: 1058 - 1072.

Otto-Bliesner, B.L., Rosenbloom, N., Stone, E.J., McKay, N.P., Lunt, D.J., Brady, E.C. and Overpeck, J.T., 2013. How warm was the last interglacial? New model-data comparisons. Philos Trans A Math Phys Eng Sci, 371(2001): 20130097.

Pal, J.S., Giorgi, F., Bi, X., Elguindi, N., Solmon, F., Rauscher, S.A., Gao, X., Francisco, R., Zakey, A., Winter, J., Ashfaq, M., Syed, F.S., Sloan, L.C., Bell, J.L., Diffenbaugh, N.S., Karmacharya, J., Konaré, A., Martinez, D., Da Rocha, R.P. and Steiner, A.L., 2007. Regional Climate Modeling for the Developing World: The ICTP RegCM3 and RegCNET. 88(9): 1395-1409.

Pascale, S., Boos, W.R., Bordoni, S., Delworth, T.L., Kapnick, S.B., Murakami, H., Vecchi, G.A. and Zhang, W., 2017. Weakening of the North American monsoon with global warming. Nature Climate Change, 7(11): 806-812.

Pascale, S. and Bordoni, S., 2016. Tropical and Extratropical Controls of Gulf of California Surges and Summertime Precipitation over the Southwestern United States. Monthly Weather Review, 144(7): 2695-2718.

Pigati, J.S., Miller, I.M., Johnson, K.R., Honke, J.S., Carrara, P.E., Muhs, D.R., Skipp, G. and Bryant, B., 2014. Geologic setting and stratigraphy of the Ziegler Reservoir fossil site, Snowmass Village, Colorado. Quaternary Research, 82(3): 477-489.

Poore, R.Z., Pavich, M.J. and Grissino-Mayer, H.D., 2005. Record of the North American southwest monsoon from Gulf of Mexico sediment cores. Geology, 33(3).

Reheis, M., J, B., SP, L., DM, M., G, S. and RJ., F., 2012. A half-million-year record of paleoclimate from the Lake Manix Core, Mojave Desert, California. . Palaeogeography, Palaeoclimatology, Palaeoecology, 365-366: 11-37.

Reynolds, R.W., Rayner, N.A., Smith, T.M., Stokes, D.C. and Wang, W., 2002. An Improved In Situ and Satellite SST Analysis for Climate. Journal of Climate, 15(13): 1609-1625.

Ritchie, E.A., Wood, K.M., Gutzler, D.S. and White, S.R., 2011. The Influence of Eastern Pacific Tropical Cyclone Remnants on the Southwestern United States. Monthly Weather Review, 139(1): 192-210.

Schneider, U., Becker, A., Finger, P., Meyer-Christoffer, A., Rudolf, B. and Ziese, M., 2011. GPCC Full Data Reanalysis Version 6.0 at 0.5°: MOnthly Land-Surface Precipitation from Rain-Gauges built on GTS-based and Historic Data.

Scussolini, P., Bakker, P., Guo, C., Stepanek, C., Zhang, Q., Braconnot, P., Cao, J., Guarino, M.-V., Coumou, D., Prange, M., Ward, P.J., Renssen, H., Kageyama, M., Otto-Bliesner, B. and Aerts, J.C.J.H., 2019. Agreement between reconstructed and modeled boreal precipitation of the Lat Interglacial. Science Advances, 5(11).

Sinha, P., Maurya, R.K.S., Mohanty, M.R. and Mohanty, U.C., 2019. Inter-comparison and evaluation of mixed-convection schemes in RegCM4 for Indian summer monsoon simulation. Atmospheric Research, 215: 239-252.

Strickland, L.E., Baker, R.G., Thompson, R.S. and Miller, D.M., 2014. Last interglacial plant macrofossils and climates from Ziegler Reservoir, Snowmass Village, Colorado, USA. Quaternary Research, 82(3): 553-566.

Sylla, M.B., Coppola, E., Mariotti, L., Giorgi, F., Ruti, P., Dell'Aquila, A. and Bi, X., 2010. Multiyear simulation of the African climate using a regional climate model (RegCM3) with the high resolution ERA-interim reanalysis. Climate Dynamics, 35: 231-247.

Turney, C.S.M. and Jones, R.T., 2010. Does the Agulhas Current amplify global temperatures during super-interglacials? Journal of Quaternary Science, 25(6): 839-843.

Velikou, K. and Tolika, K., 2017. Evaluation of the Sensitivity of the Updated RegCM4 Model to Physics Parameterizations over the Mediterranean Region: Precipitation and Temperature Simulations. Proceedings, 1(112).

Walsh, K.J., McBride, J.L., Klotzbach, P.J., Balachandran, S., Camargo, S.J., Holland, G., Knutson, T.R., Kossin, J.P., Lee, T.c., Sobel, A. and Sugi, M., 2016. Tropical cyclones and climate change. WIREs Clim Change, 7: 65-89.

Wang, B., Jin, C. and Liu, J., 2020. Understanding Future Change of Global Monsoons Projected by CMIP6 Models. American Meteorological Society.

Wang, Y.J., Cheng, H., Edwards, R.L., An, Z.S., Wu, J.Y., Shen, C.-C. and Dorale, J.A., 2001. A High-Resolution Absolute-Dated Late Pleistocene Monsoon Record from Hulu Cave, China. Science(5550): 2345-2348.

Wu, M.-L.C., Schubert, S.D., Suarez, M.J. and Huang, N.E., 2009. An Analysis of Moisture Fluxes into the Gulf of California. Journal of Climate, 22(8): 2216-2239.

Zhong, Z., Hu, Y., Min, J. and Xu, H., 2007. Numerical Experiments on the Spin-up Time for Seasonal-Scale Regional Climate Modeling. Acta Meteorologica Sinica, 21(4): 409-419.

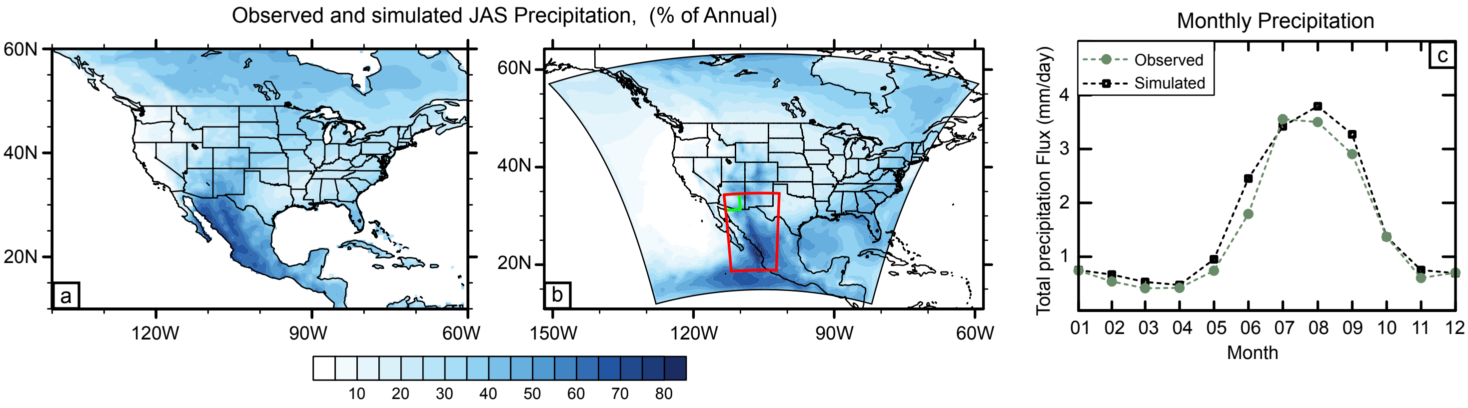

Observed and simulated JAS Precipitation, (% of Annual)
60N
40N
20N
a
120W
90W
60W
b
150W
120W
90W
60W
10
20
30
40
50
60
70
80
Monthly Precipitation
c
Observed
Simulated
Total precipitation Flux (mm/day)
1
2
3
4
01 02 03 04 05 06 07 08 09 10 11 12
Month

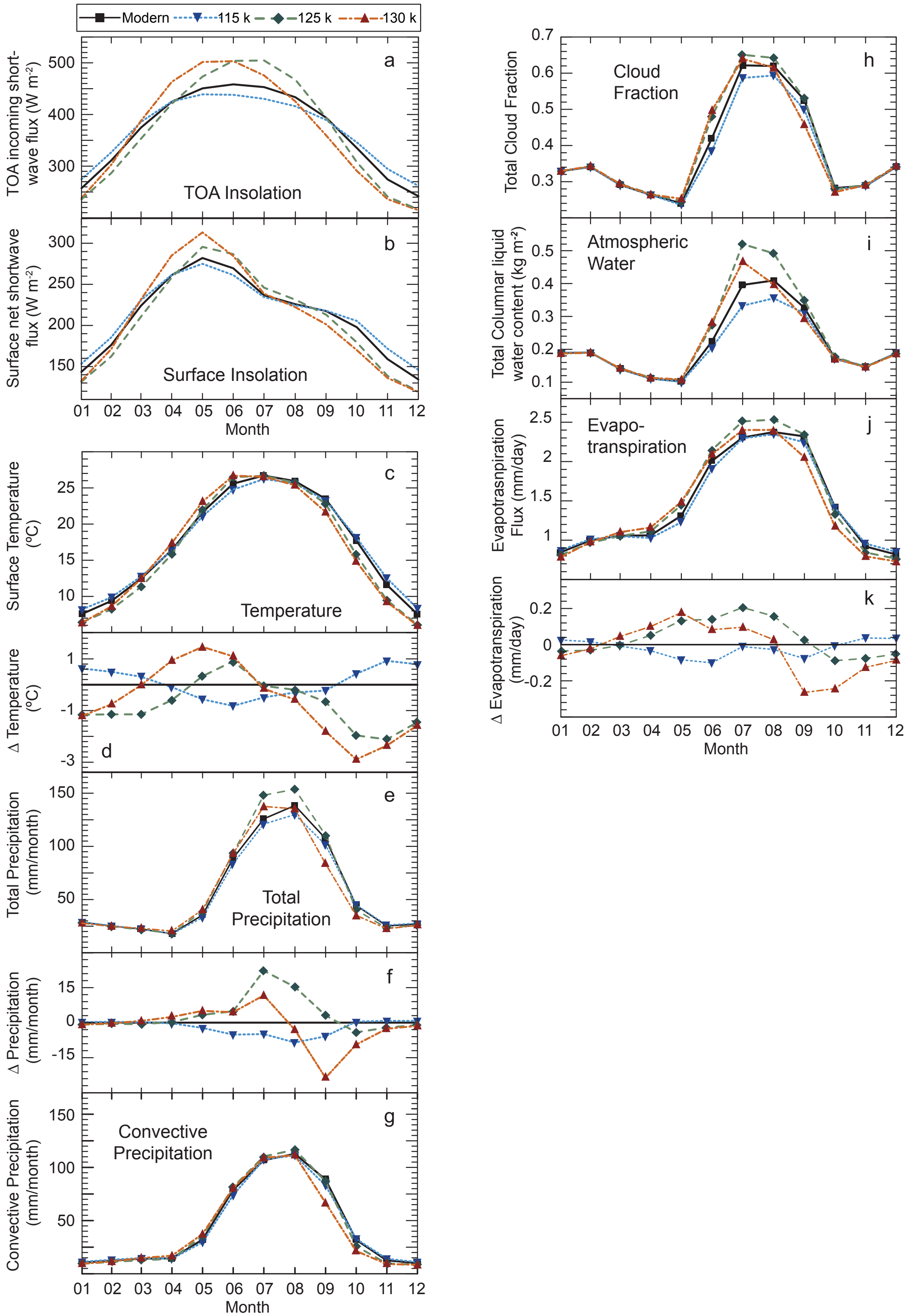

Modern
115 k
125 k
130 k
TOA incoming short-wave flux (W m⁻²)
TOA Insolation
a
Surface net shortwave flux (W m⁻²)
Surface Insolation
b
Month
Surface Temperature (°C)
Temperature
c
Δ Temperature (°C)
d
Total Precipitation (mm/month)
Total Precipitation
e
Δ Precipitation (mm/month)
f
Convective Precipitation (mm/month)
Convective Precipitation
g
Total Cloud Fraction
Cloud Fraction
h
Total Columnar liquid water content (kg m⁻²)
Atmospheric Water
i
Evapotrasnpiration Flux (mm/day)
Evapo-transpiration
j
Δ Evapotranspiration (mm/day)
k
Month

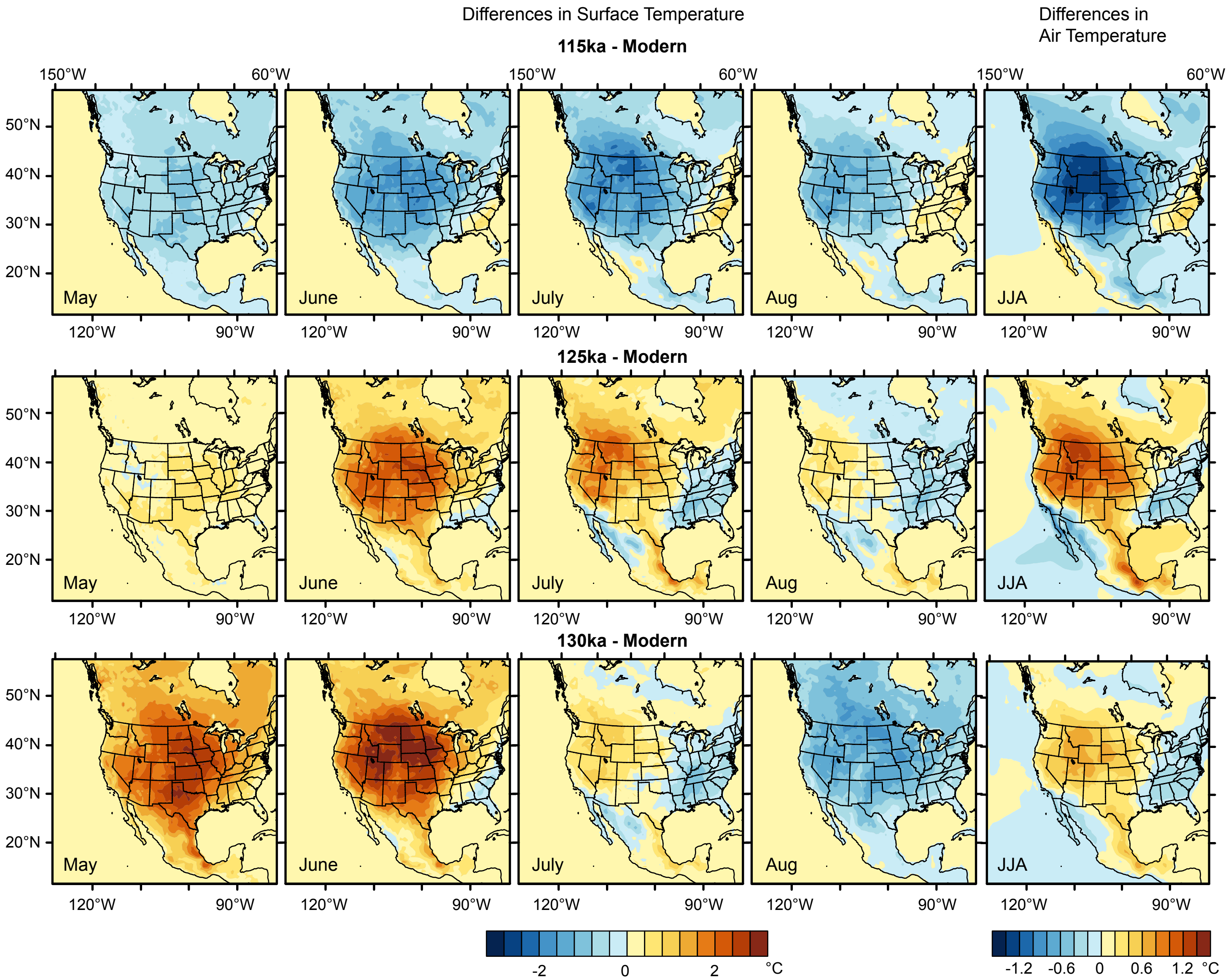

Differences in Surface Temperature
Differences in Air Temperature
115ka - Modern
125ka - Modern
130ka - Modern
150°W
60°W
120°W
90°W
50°N
40°N
30°N
20°N
May
June
July
Aug
JJA
-2
0
2
°C
-1.2
-0.6
0
0.6
1.2
°C

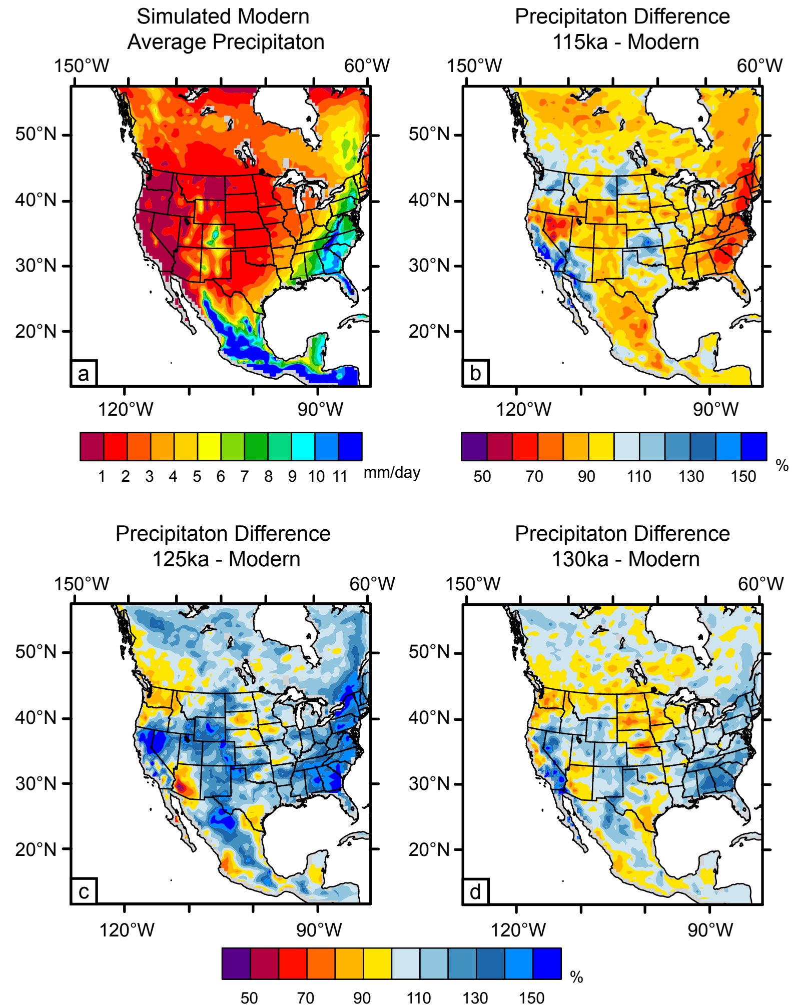

Simulated Modern
Average Precipitaton
Precipitaton Difference
115ka - Modern
Precipitaton Difference
125ka - Modern
Precipitaton Difference
130ka - Modern
150°W
60°W
50°N
40°N
30°N
20°N
120°W
90°W
a
b
c
d
1 2 3 4 5 6 7 8 9 10 11
mm/day
50 70 90 110 130 150
%

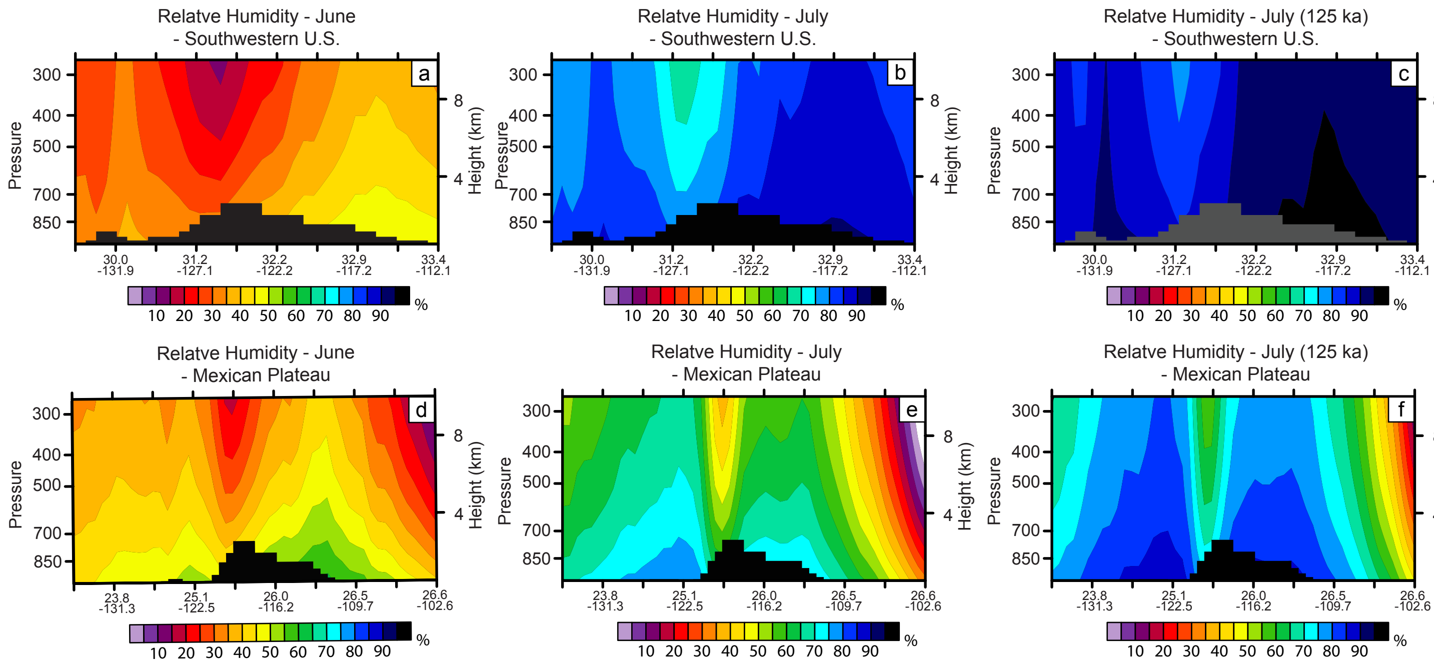

Relatve Humidity - June
- Southwestern U.S.
Relatve Humidity - July
- Southwestern U.S.
Relatve Humidity - July (125 ka)
- Southwestern U.S.
Relatve Humidity - June
- Mexican Plateau
Relatve Humidity - July
- Mexican Plateau
Relatve Humidity - July (125 ka)
- Mexican Plateau
a
b
c
d
e
f
Pressure
Height (km)
300
400
500
700
850
8
4
30.0 -131.9
31.2 -127.1
32.2 -122.2
32.9 -117.2
33.4 -112.1
23.8 -131.3
25.1 -122.5
26.0 -116.2
26.5 -109.7
26.6 -102.6
10 20 30 40 50 60 70 80 90
%

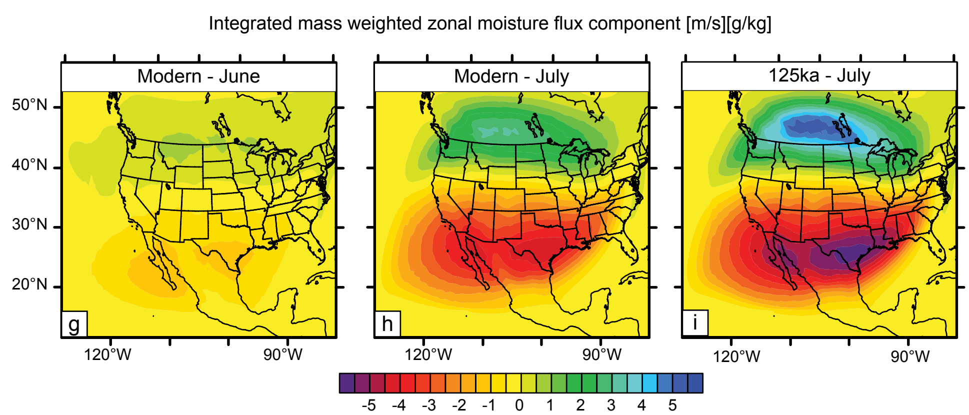

Integrated mass weighted zonal moisture flux component [m/s][g/kg]
Modern - June
Modern - July
125ka - July
50°N
40°N
30°N
20°N
120°W
90°W
g
h
i
-5 -4 -3 -2 -1 0 1 2 3 4 5

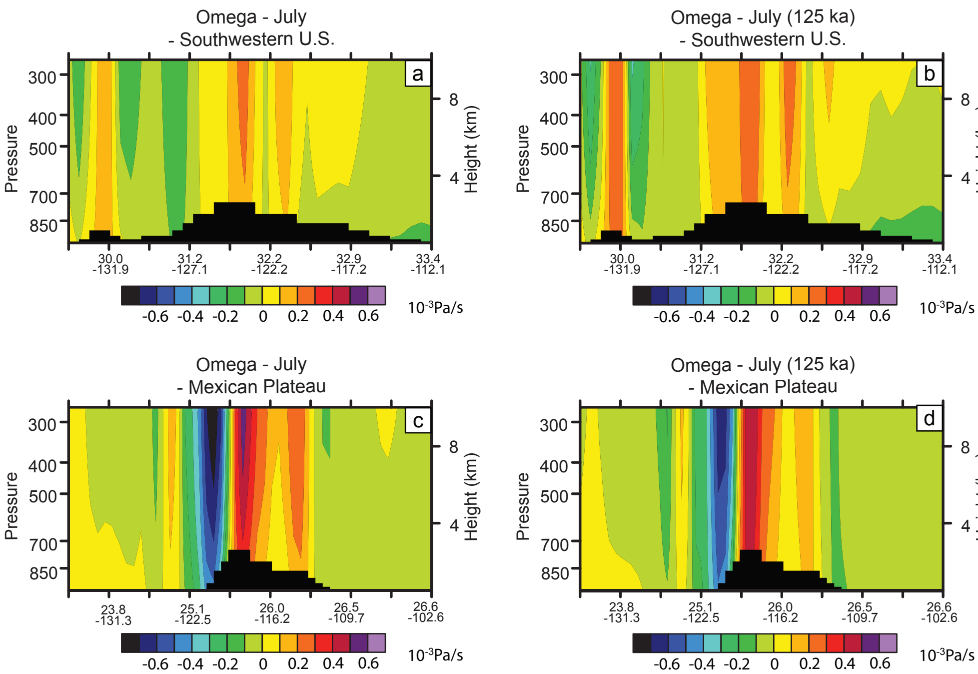
Omega - July
- Southwestern U.S.
Omega - July (125 ka)
- Southwestern U.S.
Omega - July
- Mexican Plateau
Omega - July (125 ka)
- Mexican Plateau
a
b
c
d
Pressure
Height (km)
300
400
500
700
850
8
4
30.0
-131.9
31.2
-127.1
32.2
-122.2
32.9
-117.2
33.4
-112.1
23.8
-131.3
25.1
-122.5
26.0
-116.2
26.5
-109.7
26.6
-102.6
-0.6 -0.4 -0.2 0 0.2 0.4 0.6
10-3Pa/s

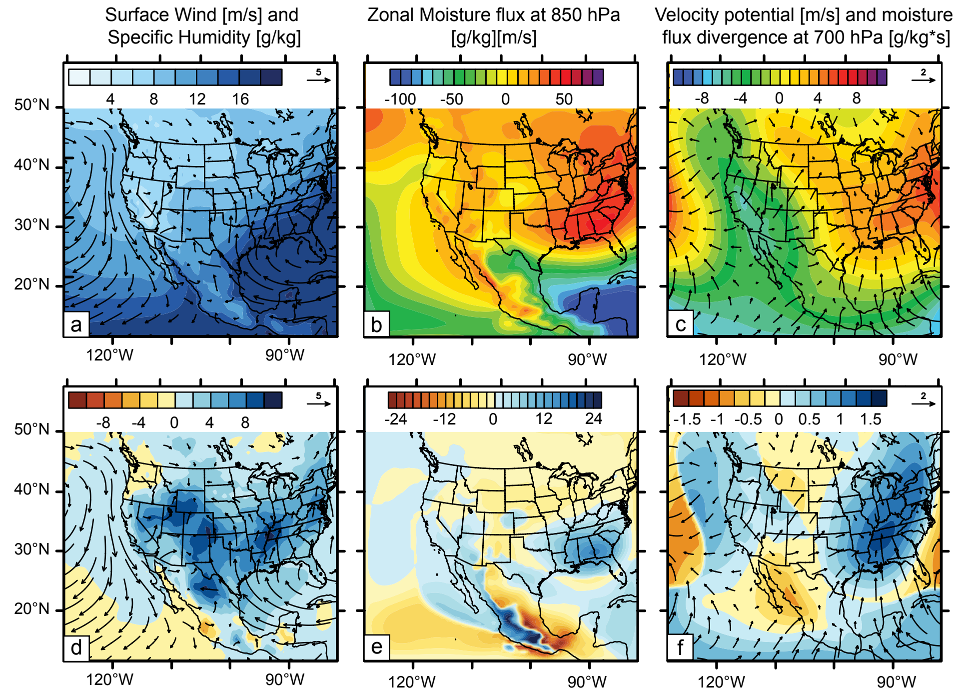

Surface Wind [m/s] and Specific Humidity [g/kg]
Zonal Moisture flux at 850 hPa [g/kg][m/s]
Velocity potential [m/s] and moisture flux divergence at 700 hPa [g/kg*s]
4 8 12 16
-100 -50 0 50
-8 -4 0 4 8
-8 -4 0 4 8
-24 -12 0 12 24
-1.5 -1 -0.5 0 0.5 1 1.5
50°N
40°N
30°N
20°N
120°W
90°W
a
b
c
d
e
f

Observed and Simulated Summer Temperature

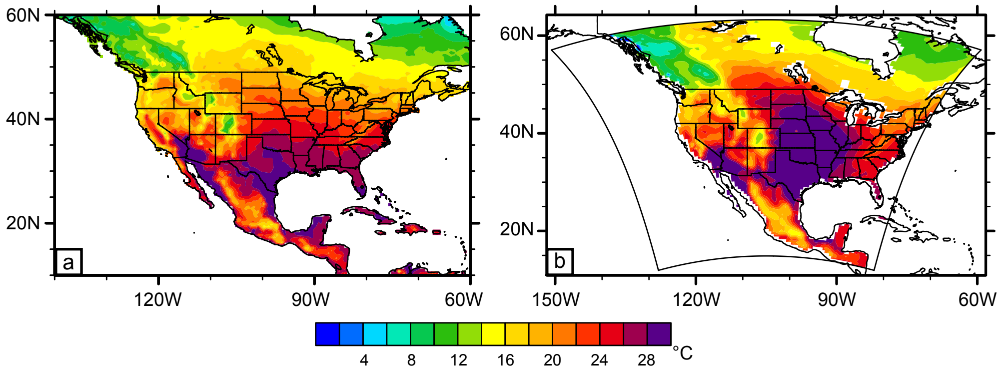

Observed and Simulated Summer Precipitation

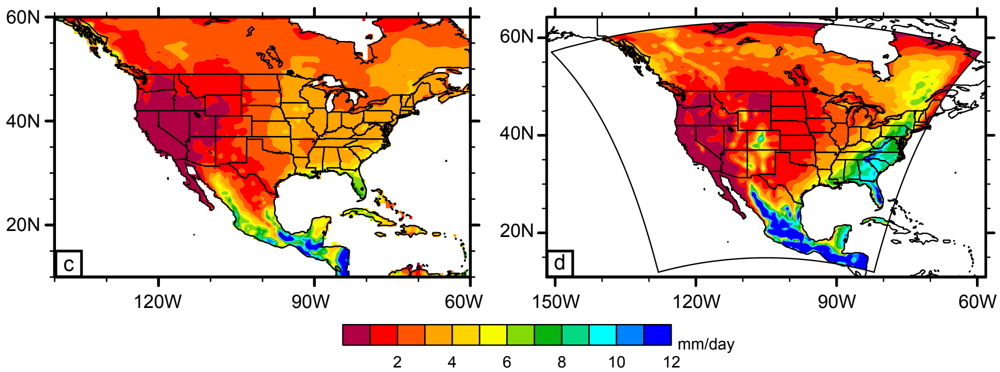

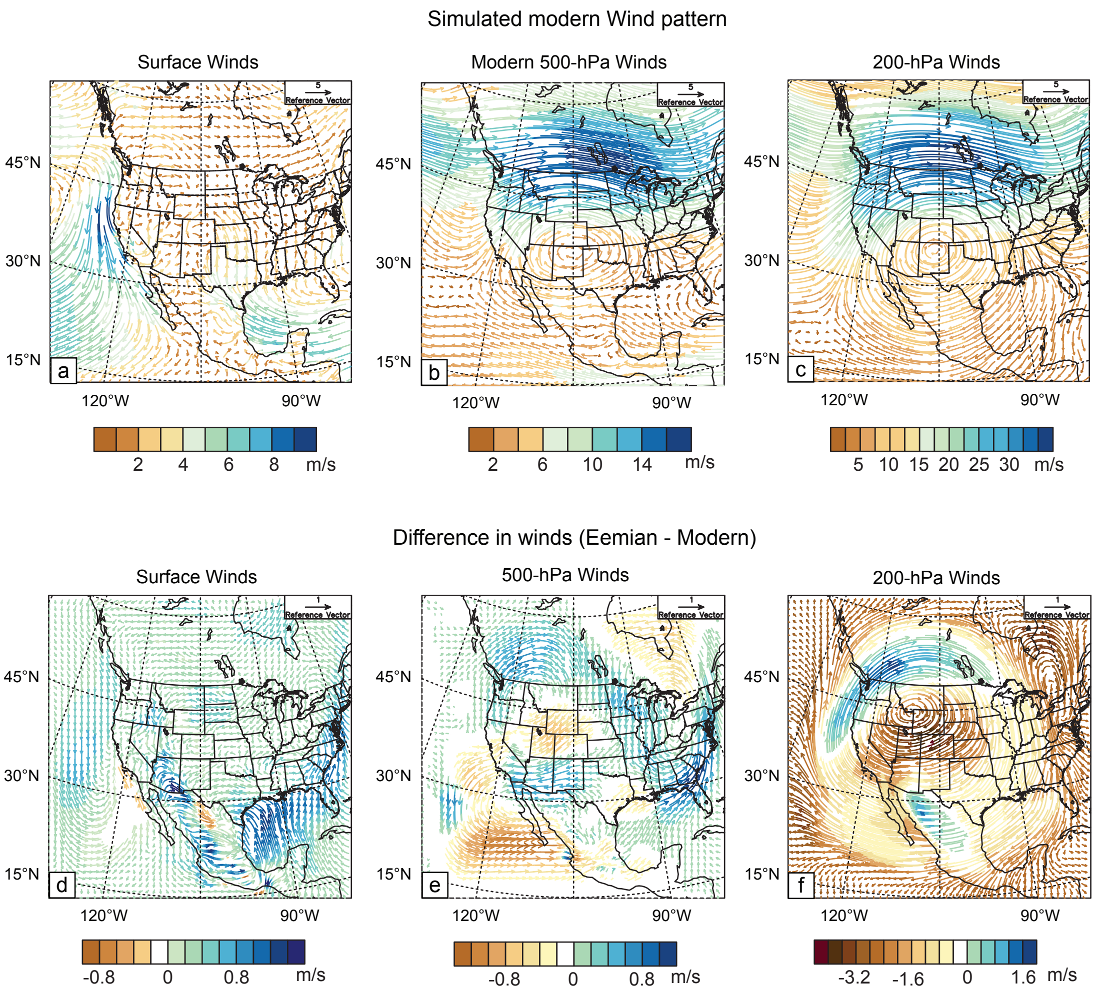

Simulated modern Wind pattern
Surface Winds
Modern 500-hPa Winds
200-hPa Winds
Reference Vector
45°N
30°N
15°N
120°W
90°W
a
b
c
2 4 6 8 m/s
2 6 10 14 m/s
5 10 15 20 25 30 m/s
Difference in winds (Eemian - Modern)
Surface Winds
500-hPa Winds
200-hPa Winds
d
e
f
-0.8 0 0.8 m/s
-0.8 0 0.8 m/s
-3.2 -1.6 0 1.6 m/s

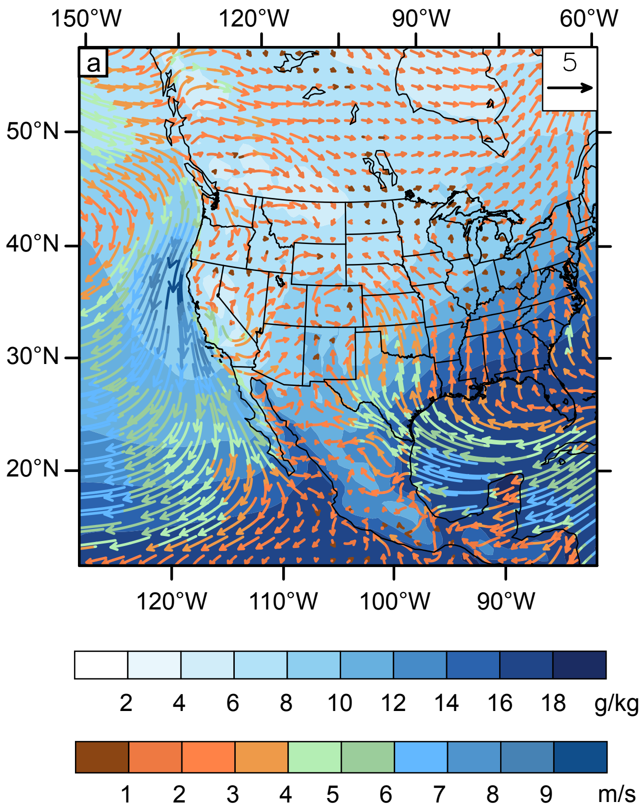

b

	modern wdsp	modern wdd	Eemian wdsp	Eemian wdd	perc
Surface winds					
Gulf of California - N	1.9	261.1	2.3	252.2	118.2
Gulf of Mexico	5.7	115.3	6.6	121.2	115.5
Western Pacific	5.6	328.3	5.1	325.3	91.5
Arizona	2.2	215.8	3.0	236.0	135.8
New Mexico	2.6	175.0	2.5	167.0	97.2
California	3.3	269.7	3.4	266.7	103.4
500 hPa winds					
Gulf of California - N	4.7	131.7	5.0	127.8	108.2
Gulf of Mexico	2.7	110.7	2.7	120.5	100.6
Western Pacific	3.4	152.9	3.4	145.8	101.3
Arizona	4.3	140.4	4.8	128.9	112.2
New Mexico	3.3	73.1	3.8	75.4	115.4
California	5.1	169.5	5.5	160.0	108.1
200 hPa winds					
Gulf of California - N	9.3	149.4	10.9	139.9	116.0
Gulf of Mexico	5.5	43.2	7.1	47.0	130.1
Western Pacific	10.3	172.1	12.1	159.3	117.4
Arizona	9.2	161.7	10.9	143.9	118.7
New Mexico	8.1	53.6	9.8	61.3	121.2
California	11.75	185.2	13.1	173.5	111.6

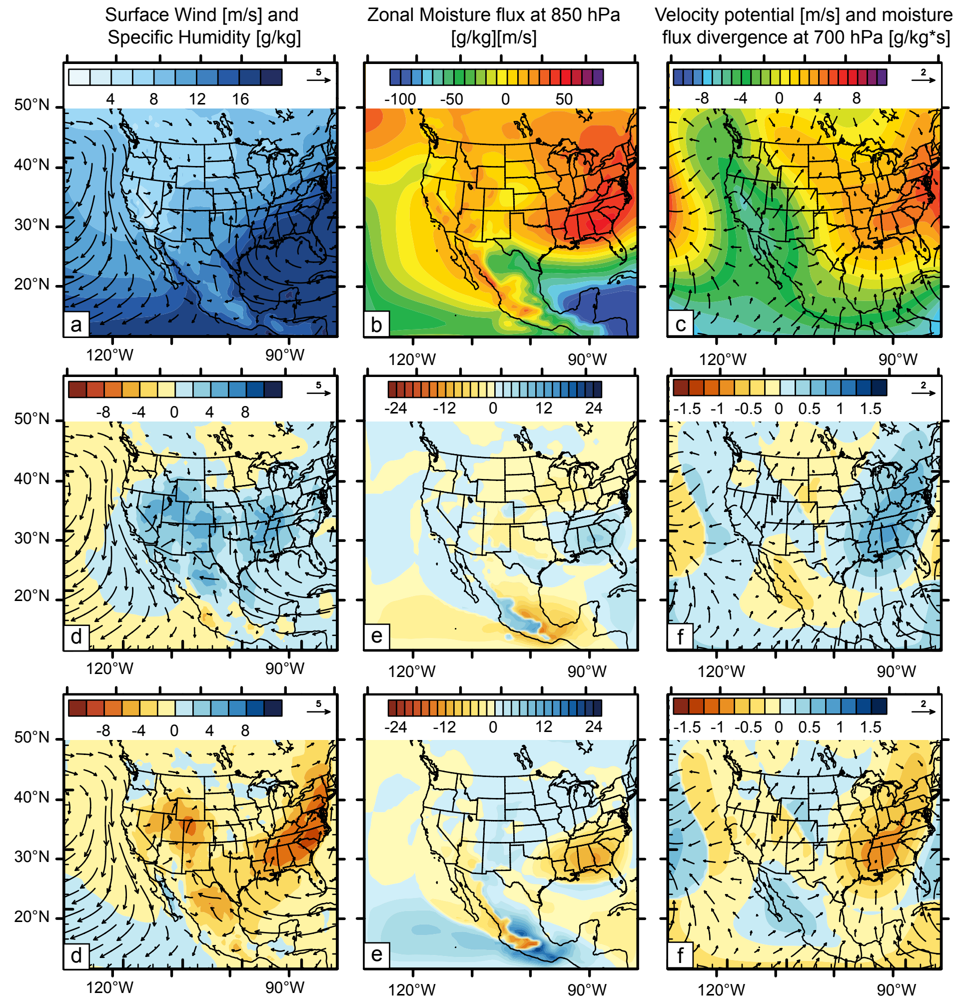
Surface Wind [m/s] and Specific Humidity [g/kg]
Zonal Moisture flux at 850 hPa [g/kg][m/s]
Velocity potential [m/s] and moisture flux divergence at 700 hPa [g/kg*s]
a
b
c
d
e
f
50°N
40°N
30°N
20°N
120°W
90°W

Table 1: Last Interglacial (LIG) forcings and boundary conditions:

Simulation	Time*	Orbital Parameters**			Trace Gases		
		ecc	obl	peri	CO2 (ppmv)	CH4 (ppbv)	N2O (ppbv)
Modern	0	0.016724	23.446	0.01636	355, 280	760	270
MinObliquity	115,000	0.043983	22.438	109.54	273	472	251
Eemian	125,000	0.042308	23.818	304.76	276	640	263
MaxObliquity	130,000	0.040129	24.247	225.73	257	512	239

Notes: *Time is in ka; **Orbital parameters are ecc = eccentricity, obl = obliquity, and peri = presession (Berger and Loutre); Trace gases are from http://www.ncdc.noaa.gov/paleo/icecore.html